3-D MHD SIMULATIONS OF CMES BY COUPLED CORONAL AND HELIOSPHERIC MODELS

D. Odstrcil [*1], J. A. Linker[2], R. Lionello[2], Z. Mikic[2], P. Riley[2], V. J. Pizzo[3], and J. G. Luhmann[4]

[1]University of Colorado, CIRES-NOAA/SEC, Boulder, CO 80305, USA
[2]Science Applications International Corporation, San Diego, CA 92121, USA
[3]NOAA/Space Environment Center, Boulder, CO 80305, USA
[4]Space Science Laboratory, University of California, Berkeley, CA 94720, USA

ABSTRACT

Merging of coronal and heliospheric magnetohydrodynamic (MHD) models is demonstrated for a 3-D idealized case involving a magnetic flux rope, shock, streamer belt, and current sheet. The disruption of a sheared helmet streamer launches a coronal mass ejection (CME, simulated by the coronal model), which evolves during its propagation through interplanetary space (simulated by the heliospheric model). These models employ different physical approximations and numerical grids to simulate physical phenomena over their respective spatial and temporal domains. The coupled simulation enables self-consistent tracking of transient disturbances from their origin in the solar atmosphere to their geo-effective consequences at the Earth.

Key words: coronal mass ejection, magnetic flux rope, solar wind, interplanetary shock, magnetohydrodynamic model, numerical simulation.

1. INTRODUCTION

Space weather research and forecasting involves a complex chain of various dynamic phenomena occurring simultaneously on different spatial and temporal scales. Coronal mass ejections (CMEs) and their interplanetary consequences (ICMEs) represent different aspects of the same phenomenon responsible for large geo-magnetic storms (*Gosling,* 1990). Because of the great complexity these individual aspects have typically been investigated separately. This approach is useful for revealing the basic underlying physics; however, a complete picture requires a comprehensive model of all of the processes considered together. Recently, we have successfully merged two-dimensional magnetohydrodynamic (MHD) coronal and heliospheric models (*Odstrcil et al.,* 2002). In this paper, we demonstrate the merging of these models for a three-dimensional (3-D) idealized case involving a magnetic flux rope, shock, streamer belt, and current sheet.

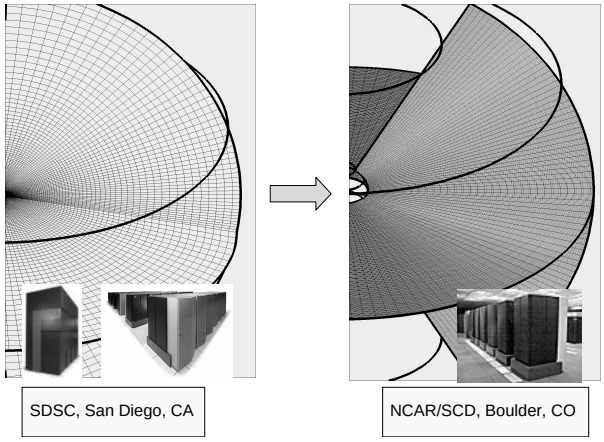

Figure 1. Merged numerical grids. Coronal model computations are performed on a non-uniform mesh, with $101 \times 101 \times 128$ *grid points, between 1 and 30* R_S *shown at the left. Heliospheric model computations are performed on a uniform mesh with* $256 \times 120 \times 180$ *grid points, between 30 and 275* R_S *shown at the right. The output from the coronal model at 30* R_S *is used as input for the heliospheric model. Superimposed are images of the computer facilities at the respective supercomputer centers.*

2. NUMERICAL MODELS

We distinguish between the "coronal" region, which ranges from the photosphere up to 30 R_S, and the "heliospheric" region, which covers the region of space between 30 and 275 R_S (Figure 1). The coronal region involves more complex physical processes

[*]on leave from the Astronomical Institute, Academy of Sciences of the Czech Republic, 25165 Ondřejov, Czech Republic

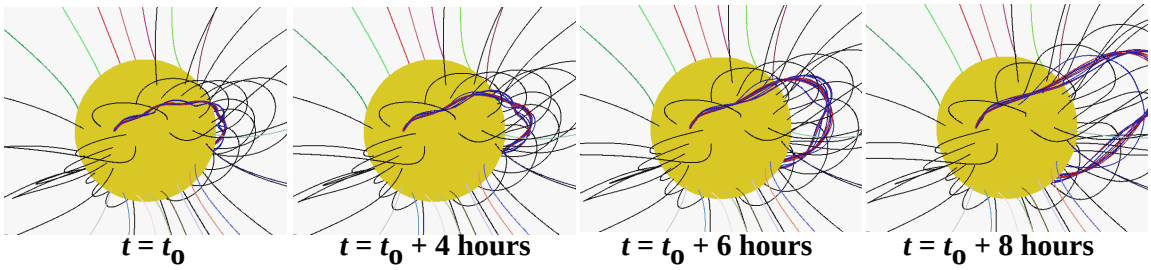

Figure 2. Three-dimensional simulation of the eruption of a helmet streamer resulting from the emergence of magnetic flux.

and the MHD equations involve the plasma electric resistivity and kinematic viscosity. In the heliospheric region the ambient solar wind flow is everywhere super-critical and the MHD equations describe an ideal plasma. Computationally, it is more efficient to advance the heliospheric portion of the simulation independently of the coronal time step.

The coronal model is based on the 3-D resistive MHD equations that are solved by a semi-implicit finite-difference scheme using staggered values (*Mikic and Linker,* 1994; *Linker and Mikic,* 1995; *Linker et al.,* 2001). The coronal model uses a ratio of specific heats $\gamma = 1.05$ to crudely simulate heat conduction processes and thermal energy sources. The heliospheric model is based on the 3-D ideal MHD equations that are solved by an explicit finite-difference TVDLF scheme using cell-centered values (*Odstrcil at al.,* 1996; *Toth and Odstrcil,* 1996; *Odstrcil and Pizzo,* 1999a,b). The heliospheric model uses $\gamma = 5/3$ to describe the fully-ionized solar wind plasma and produces accurate shock strengths.

The output from the coronal model consists of a temporal sequence of MHD flow parameters, which are used as a boundary condition for the heliospheric solutions. Our scheme stores values on two contiguous spherical surfaces in the upper corona, yielding both values and gradients for a guard-cell approach on the inner boundary of the heliospheric model. No solar rotation is imposed in the coronal model. Magnetic field components at the heliospheric inner boundary are, however, adjusted to account for solar rotation. It is assumed that the magnetic field lines are frozen to the flow by the high electrical conductivity and corotate with the mean azimuthal velocity $V_{\rm rot}$. This effect contributes to the steady background flow by an azimuthal field component

$$B_\varphi = B_\varphi^c - B_r \sin(\theta) V_{\rm rot}/V_r \ ,$$

where B_φ^c is the azimuthal component resulting from coronal computations of the azimuthal shearing.

3. RESULTS AND DISCUSSION

The coronal simulation starts from an initial potential magnetic field and a spherically symmetric Parker solar wind. The magnetic flux distribution was chosen to yield a streamer belt that is slightly below and inclined to the solar equatorial plane. The resulting heliospheric configuration consists of a dense and slow streamer belt flow near the equatorial plane surrounded by less dense and faster streams in the northern and southern hemispheres. The heliospheric streamer belt has an embedded heliospheric current sheet, and it is about 10% denser and 50 km/s slower than the fast streams. This is a relatively low contrast, which will be improved by incorporation of more realistic heating in the solar corona in future simulations.

Once the ambient state is established, a shear flow near the neutral line is applied to feed magnetic energy into the streamer (*Amari et al.,* 2000; *Linker at al.,* 2001). This shear flow is not intended to model actual flows on the Sun; it is just a convenient mechanism for producing strongly sheared field lines that are nearly aligned with the neutral line. Then a reduction in the magnetic flux (flux cancellation) is imposed near the sheared arcade configuration and leads to the formation of a magnetic flux rope. When the flux cancellation reaches a critical threshold, the entire configuration erupts with the release of a considerable amount of magnetic energy as shown in Figure 2.

The solar eruption evolves into a traveling interplanetary disturbance that significantly exceeds its original angular size (Figure 3). As with our previous 2-D simulation (*Odstrcil et al.,* 2002), the helmet streamer is destroyed by the eruption of the flux rope. This causes the magnetic field and mass contained in the streamer to be ejected into the heliosphere (see also *Wu et al.,* 1999). The streamer returns to its original configuration after the passage of the CME. The flux rope preserves its basic configuration as it evolves into the magnetic cloud detected at 1 AU (see also *Vandas et al.,* 2002).

The ejected coronal mass generates MHD waves that steepen into a shock that propagates into the structured solar wind. A portion of the transient disturbance interacts with the slow, dense streamer belt flow. A dimple forms within the shock front, but not within the ejected mass, due to strong magnetic fields in the flux rope (Figures 4 and 5). The flux rope is compressed but resists local distortion; however, it does evolve into a lense-like shape in the meridional cross section (see also *Odstrcil et al.,* 2002). The dis-

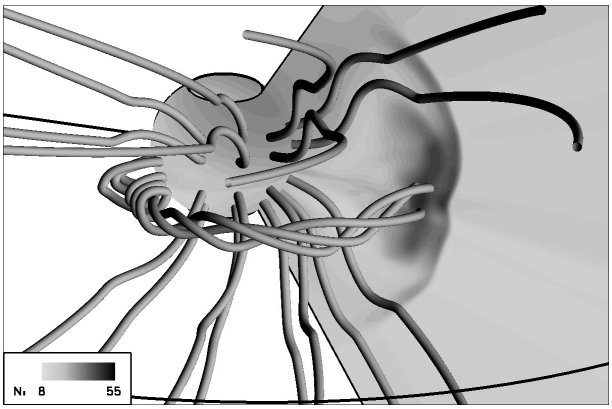

Figure 3. Global view of the magnetic flux rope expanding into interplanetary space. Selected magnetic field lines are shown in 3-D and the plasma number density (normalized to 1 AU; grey shading) is shown in the meridional plane and at the heliospheric inner boundary.

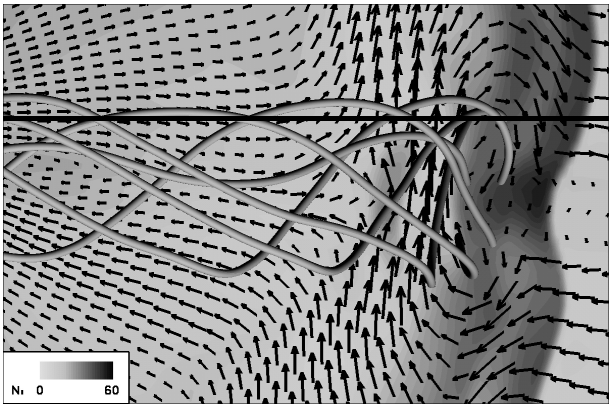

Figure 4. Detailed view of the magnetic flux rope. Selected magnetic field lines are shown in 3-D. The plasma number density (normalized to 1 AU; grey shading) and magnetic field vectors are shown in the meridional plane. The thick horizontal line is the equatorial plane.

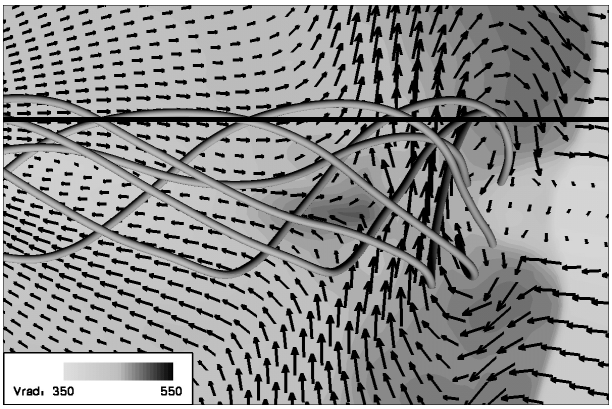

Figure 5. The same as in Figure 3 but for the flow velocity (km/s).

tortion is expected to be greater for larger differences between slow and fast streams (see *Riley et al.,* 1997; *Odstrcil and Pizzo,* 1999a). Density and velocity enhancements trailing the flux rope are signatures of the jetted outflow, driven by post-eruptive reconnection underneath the flux rope, as suggested by *Riley et al.* (2002).

An interesting effect happens with interplanetary magnetic field lines behind the traveling ICME (Figure 6). The field lines are stretched out and the magnetic field is oriented nearly radial to the Sun over a large domain (i.e., it can be observed for substantial period of time). This effect is caused by rarefaction waves trailing the ICME and it is similar to the origin of radial magnetic fields at declining solar wind flow speeds described by *Gosling and Skoug* (2002).

For propagation of energetic particles, it is important to know the connectivity of the magnetic field lines intersecting any particular observing point (Figure 7). Initially all field lines are open (i.e., they are connected to the Sun at one end) except those near the current sheet which may reconnect and form loops. As the disturbance propagates through interplanetary space, the field lines can be disconnected (both ends connecting to open space) or they can be part of the flux rope with both ends connected to the Sun.

4. CONCLUSIONS

The idealized calculations presented here are intended to illustrate that it is possible to perform self-consistent MHD calculations of Sun-to-Earth space weather events. Merged coronal and heliospheric models allow us to follow the consequences of solar activity directly and more realistically. In coupled coronal and heliospheric simulations, the interplanetary transient disturbance is generated by a magnetic eruption in the solar corona. Such disturbances are self-consistent with the surrounding solar wind parameters *ab initio*. This is especially important for investigation of more realistic scenarios involving a structured solar wind with a heliospheric current sheet.

In general, our 3-D results are similar to previous 2-D results (*Odstrcil at al.,* 2002) but the evolution of the magnetic field is more complicated. Dynamic phenomena include field-line draping by the traveling and expanding ICME, and distortion of a shock at the heliospheric plasma sheet with embedded heliospheric current sheet. The 3-D distribution of interplanetary magnetic field is important for propagation of energetic particles and for initiation of geomagnetic storms (*Odstrcil and Pizzo,* 1999b).

Increasing the resolution beyond that used in the present simulation is not likely to change the global picture significantly. However, increased resolution is necessary when we tackle more realistic scenarios in the future, such as reconnection, shock structure interaction, details of magnetic flux rope, etc. Work

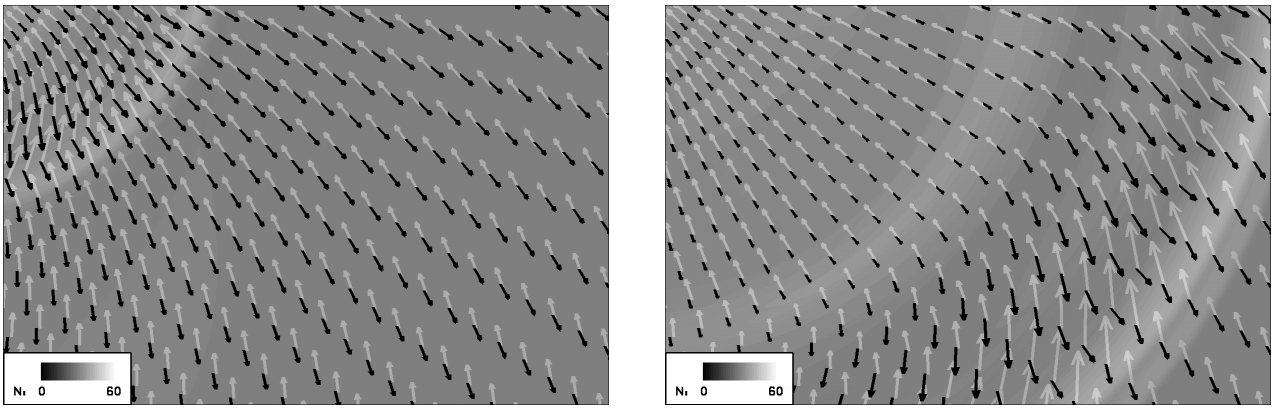

Figure 6. The transient disturbance propagating through interplanetary space at two different times. Shading corresponds to the plasma density normalized to 1 AU (larger values correspond to lighter colors). Vectors of the magnetic field are shown at $\theta = 70°$ (dark) and $110°$ (light).

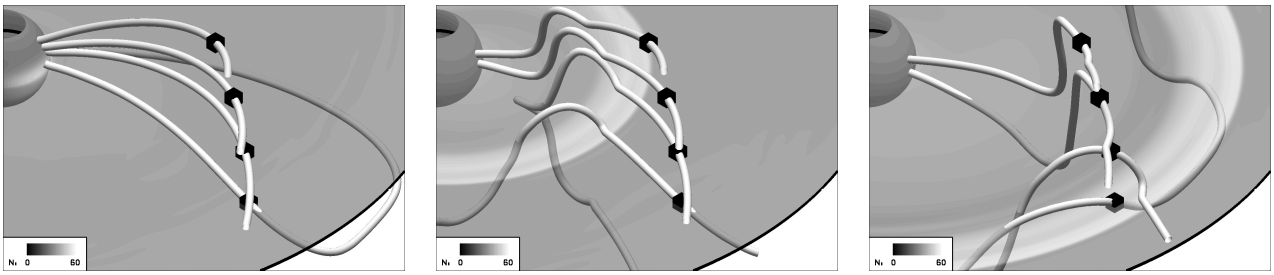

Figure 7. Connectivity of interplanetary magnetic field lines at three different times. Shading corresponds to the plasma density normalized to 1 AU (larger values correspond to lighter colors). Magnetic field lines are shown for observing points at 1 AU, $\varphi = 180°$, and $\theta = 60°$, $70°$, $80°$, and $90°$.

is in progress toward more accurate physical models, coupling procedures, analyses of results, and comparisons with observations.

ACKNOWLEDGMENTS

This work was supported by NSF ATM000950 grant and NSF Center for Integrated Space Weather Modeling. Additional support was from NASA Sun-Earth Connection Theory and Supporting Research and Technology Programs and by grant A3003003 from the Academy of Sciences of the Czech Republic. Computational facilities were provided by National Center for Atmospheric Research in Boulder and San Diego Supercomputer Center in San Diego.

REFERENCES

Amari, T., J. F. Luciani, Z. Mikic, and J. Linker, *Astrophys. J., 529,* L49-L52, 2000.

Gosling, J. T., Coronal mass ejections and magnetic flux ropes in interplanetary space, in *Physics of Magnetic Flux Ropes, Geophys. Monogr. Ser.,* vol. 58, edited by C. J. Russell, E. R. Priest, and L. C. Lee, pp. 343-364, AGU, Washington, D.C., 1990.

Gosling, J. T., and R. M. Skoug, *Geophys. Res. Letts., submitted,* 2002.

Linker J. A., and Z. Mikic, *Astrophys. J., 438,* L45-L48, 1995.

Linker, J. A., R. Lionello, Z. Mikic, and T. Amari, *J. Geophys. Res., 106,* 25,165-25,176, 2001.

Mikic, Z., and J. A. Linker, *Astrophys. J., 430,* 898-912, 1994.

Odstrcil, D., M. Dryer, and Z. Smith, *J. Geophys. Res., 101,* 19,973-19,984, 1996.

Odstrcil, D., and V. J. Pizzo, solar wind flow 1. CME launched within the streamer belt, *J. Geophys. Res., 104,* 483-492, 1999a.

Odstrcil, D., and V. J. Pizzo, *J. Geophys. Res., 104,* 28,225-28,239, 1999b.

Odstrcil, D., J. A. Linker, R. Lionello, Z. Mikic, P. Riley, V. J. Pizzo, and J. G. Luhmann, *J. Geophys. Res., in press,* 2002.

Riley, P., J. T. Gosling, and V. J. Pizzo, *J. Geophys. Res., 102,* 14,677-14,685, 1997.

Riley, P., J. A. Linker, Z. Mikic, D. Odstrcil, V. J. Pizzo, and D. F. Webb, *Astrophys J. in press,* 2002.

Toth, G., and D. Odstrcil, *J. Comput. Phys., 128,* 82-100, 1996.

Vandas, M., D. Odstrcil, and S. Watari, solar wind, J. Geophys. Res., in press, 2002.

Wu, S. T., W. P. Guo, D. J. Michels, and L. F. Burlaga, *J. Geophys. Res., 104,* 14,789-14,802, 1999.